Assessing the Increase in Specific Surface Area for Electrospun Fibrous Network due to Pore Induction

Konstantinos Alexandros G. Katsogiannis[a,], Goran T. Vladisavljević[a], Stella Georgiadou[a], Ramin Rahmani[b]*

[a] *Department of Chemical Engineering, Loughborough University, Loughborough, Leicestershire, LE11 3TU, UK*

[b] *Wolfson School of Mechanical, Electrical and Manufacturing Engineering, Loughborough University, Loughborough, Leicestershire, LE11 3TU, UK*

** email K.A.Katsogiannis@lboro.ac.uk*

Abstract

The effect of pore induction on increasing electrospun fibrous network specific surface area was investigated in this study. Theoretical models based on the available surface area of the fibrous network and exclusion of the surface area lost due to fibre-to-fibre contacts, were developed. The models for calculation of the excluded area are based on Hertzian, Derjaguin-Muller-Toporov (DMT) and Johnson-Kendall-Roberts (JKR) contact models. Overall, the theoretical models correlated the network specific surface area to the material properties including density, surface tension, Young's modulus, Poisson's ratio as well as network physical properties such as density and geometrical characteristics including fibre radius, fibre aspect ratio and network thickness. Pore induction proved to increase the network specific surface area up to 52%, compared to the maximum surface area that could be achieved by non-porous fibre network with the same physical properties and geometrical characteristics. The model based on Johnson-Kendall-Roberts contact model describes accurately the fibre-to-fibre contact area under the experimental conditions used for pore generation. The experimental results and the theoretical model based on Johnson-Kendall-Roberts contact model show that the increase in network surface area due to pore induction can reach to up to 58%.

Keywords: Electrospinning, Fibrous network; Porous fibre; Specific surface area; Pore induction; Contact mechanics

Nomenclature

a	Radius of the circular contact area
d	Diameter of the fibre
E	Young's modulus elasticity for the fibre material
E^*	Reduced Young's modulus of elasticity for the contact
F_c	Applied force at the contact (contact load)
F_{av}	Average force applied on each layer
F_c	Force at each individual contact
g	Gravitational acceleration
L	Sum of the length of fibres
L_i	Length of each individual fibre
m	Mass
N_{con}	Number of contacts
n	Number of layers
n_f	Number of fibres ion the network
R	Radius of curvature
R_e	Equivalent radius of curvature
R_{rc}	Reduced radius of curvature
R_s	Radius of sphere
S_{excl}	Excluded area due to each contact
S_{max}	Maximum available surface area
S_{net}	Net specific surface area
t	Thickness of fibrous mat
w_l	Weight of each layer
w_t	Total weight

Greek Symbols

A, B	Intermediate variables

γ	Surface tension
Δ	Total local deflection at the contact patch
ε	Porosity of the fibrous network
Θ	Orientation angle factor
θ	Angle between cylinders with different orientation
λ	Fibre aspect ratio
v	Poisson's ratio
ρ	Density of network
ρ_m	Density of material

Abbreviations

DMT	Derjaguin-Muller-Toporov
JKR	Johnson-Kendall-Roberts
NIPS	Non-solvent Induced Phase Separation
PCL	poly ε-caprolactone
SSA	Specific Surface Area

1. Introduction

Electrospinning is a straightforward method for the production of polymer fibres with diameters down to the nanometre scale[1]. During this process a polymer solution is accelerated towards a grounded collector under forces applied by an electric field. The stretching of the macromolecular chains, caused by the repulsive forces between homonymous charges and the simultaneous solvent evaporation lead to the deposition of ultrathin fibres on the collector. One of the main advantages of the produced fibres is their high Specific Surface Area (SSA). Hence, those materials are becoming popular in applications like filtration[2] or catalysis[3], where higher values of SSA are of importance.

Porosity induction is generally considered as an effective method for increasing the SSA of any material. Thus pore generating methods, such as the use of humidity[4] and phase separation[5] have been successfully combined with electrospinning for the

production of porous polymer fibres. Even though, generally, networks composed of porous fibres seem to possess higher SSA than networks composed by non-porous fibres[6], an accurate evaluation of the pore induction efficiency in terms of network SSA increase is scarce in the literature. Acquiring such knowledge can be extremely useful in evaluating the efficiency of different proposed methodologies (e.g. pore induction or fibre diameter reduction) for increasing the network SSA. A common approach that has been implemented is the comparison between SSAs of networks produced under the same experimental conditions independent of the pore generating mechanism[7]. However, in addition to fibre porosity, other properties that contribute in the configuration of the network SSA (fibre diameter and network density) were also different in the samples. Thus, such an approach can only be used for evaluating the efficiency of the pore generating mechanism in increasing the network SSA. Furthermore, the lack of ability to simultaneously control both fibre diameter and network density, highlights the necessity for use of theoretical modelling to help quantify SSA values for a given fibre network. Upon examining the relevant literature, theoretical works such as that of Eichhorn and Sampson[8], which use statistical approaches to predict the electrospun network SSA. Nevertheless, those methods do not include contact mechanics models for more accurate quantification of the network SSA. Therefore, there seems to be a requirement for further improving of the existing statistical models through combining with existing contact mechanics models.

The dual aim of this study is to verify the fibrous network SSA increase due to pore induction and subsequently, quantify the associated SSA values. In this study, the statistical approach is combined with available theories in contact mechanics for the development of appropriate theoretical model; correlating the fibrous network SSA to readily measurable characteristics. In doing so, three different contact models are considered in this study. The model that most accurately predicted the network SSA was selected based on experiment results for networks composed of non-porous fibres. Finally, the calculation of the rise in network SSA due to pore induction was performed through comparison between the theoretically predicted SSA of a network composed of non-porous fibres to the experimentally measured SSA of a network composed of porous fibres with the same physical properties and geometrical characteristics. The polymer used in this study was poly (ε-caprolactone) (PCL) and

a combinative electrospinning-Non-solvent Induced Phase Separation (NIPS) technique was used for the production of porous fibres[9]. The approach presented in this study provides a more detailed analysis of the individual factor contribution in the configuration of an electrospun network SSA compared to the existing models.

2. Theoretical Analysis

2.1. Net specific surface area

A description of the phenomenological processes occurring within the fibrous network can facilitate understanding of the principles based upon which the theoretical model is developed. The network SSA is created by the fibre bodies. The individual fibre characteristics determine the maximum available network SSA. However, the individual fibre-to-fibre contacts within the network decrease the actual SSA. Each contact deducts from a given amount of the overall network SSA, hence is the deviation from the maximum available network SSA. To determine the excluded area two parameters should be specifically determined: number of the fibre-to-fibre contacts and the contact area at each individual contact point. Therefore, the net specific surface area, S_{net}, can be expressed as follow:

$$S_{net} = S_{max} - N_{con}\, S_{excl} \quad (1)$$

where, S_{max}, N_{con} and S_{excl} stand for maximum available surface area, the number of fibre-to-fibre contacts within the network and the area excluded due to each contact, respectively.

2.2. Maximum available specific surface area of the fibrous network

The maximum available network SSA is calculated based on the assumption that all the fibres constructing the network are cylinders of equal radius R with individual length L_i. Thus, the maximum network SSA can be written as follow:

$$S_{max} = 2\pi R \sum_{i=1}^{n_f} L_i + 2\pi R^2 n_f \quad (2)$$

where, n_f is the number of fibres from which the network is composed of.

Normally, the length of the fibres is significantly larger than their radius (typically the ratio L_1/R is much higher that 1000[10]), therefore equation (2) can be simplified to:

$$S_{max} = 2\pi RL \quad (3)$$

where, $L = n_f L_i$ is the sum of the length of the fibres in the network.

Considering the density of fibre material, ρ_m, and the volume of a cylinder, the maximum network SSA (per unit mass) can be calculated as:

$$\frac{S_{max}}{m} = \frac{2}{\rho_m R} \quad (4)$$

Equation (4) demonstrates that the maximum SSA of a fibrous network (achievable when no fibre-to-fibre contact occurring within the network), composed of smooth surface fibres, is proportional to the reciprocal of fibre radius, R and material density, ρ_m.

2.3. Number of fibre-to-fibre contacts

Studies that use statistical approaches for calculation of the number of fibre-to-fibre contacts within a fibrous network are available in the literature (e.g. see Eichhorn and Sampson[11]). Nevertheless, the work of Bagherzadeh et al[12] was selected for adaptation in this study, since they more realistically exclude the fibre length occupied by previous contacts prior calculating the probability for any further contact.

According to that study, the average number of contacts per unit fibre mass in a multi-layer fibrous network is:

$$N_{cont} = (2n-1)\frac{2\log(1/\varepsilon)}{\pi+8\lambda\log(1/\varepsilon)}\frac{1}{\rho_m R^3} \quad (5)$$

where, ε is the porosity of the fibrous network, λ is the fibre aspect ratio, n is the number of layers in the network and t is the thickness of the fibrous mat. Those parameters mentioned above are given as follow, respectively:

$$\varepsilon = 1 - \frac{\rho}{\rho_m} \quad (6)$$

$$\lambda = \frac{L}{2R} \quad (7)$$

$$n = \frac{t}{2R} \quad (8)$$

2.4. Contact area based on Hertzian model

In the absence of any dynamic structural vibrations of the fibre network, based on the Hertzian contact theory, the contact area between two elastic bodies with convex surface profile is determined by four parameters[13]: the material from which the bodies are made, the normal force applied on the bodies, the size of the bodies, the shape of the bodies and finally their orientation with respect to each other.

In the case of fibrous network, the contact can be easily assumed that occurs between two cylinders. However, before proceeding further with the analysis of contact between two cylinders, for the ease of understanding, it might be easier to consider the contact between two spheres at the first instance. The contact area of two spheres with equal radii R_s is a circle, as shown in Figure 1.

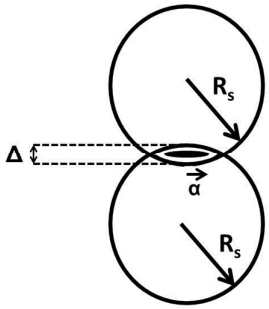

Figure 1: Schematics of contact between two spheres with equal radii. The contact area is the black shaded area.

The maximum local displacement of the spheres at the contact footprint is given by:

$$\Delta = \frac{a^2}{R_{rc}} \quad (9)$$

where, a is the radius of the circular contact area and R_{rc} is the reduced radius of curvature, which for the contact of spheres of equal radius R_s, is given as follow:

$$\frac{1}{R_{rc}} = \frac{2}{R_s} \quad (10)$$

The radius of the circular contact area, a can be calculated by:

$$a = \left(\frac{3F_c R_{rc}}{4E^*}\right)^{1/3} \quad (11)$$

where, F_c is the applied force at the contact and E^* is the reduced Young's modulus of elasticity for the contact, which for spheres made by the same material is given by:

$$\frac{1}{E^*} = 2\frac{1-\nu^2}{E} \quad (12)$$

where, E and ν are Young's modulus of elasticity and Poisson's ratio of the sphere material, respectively.

In the case of the fibrous network, the contact occurs between randomly oriented cylinders. The issue, however, can be simplified by employing the methodology described by Bhushan[13] for calculating the equivalent radius of contact for two cylinders which are in different orientations. The basis for that is the change of the coordinates of set of axes formed by the cylinders. The new set of axes for two cylinders of the same radius has to meet the requirement of:

$$\mathrm{A} + \mathrm{B} = \frac{1}{R} \quad (13)$$

$$\mathrm{B} - \mathrm{A} = \frac{1}{\sqrt{2}R}\sqrt{1 + \cos 2\theta} \quad (14)$$

where, R is the radius of the cylinders and θ is the angle formed by them due to the difference in their orientations.

The equivalent radius of curvature, R_e, is then calculated by the following relationship:

$$R_e = \frac{1}{2}(\mathrm{AB})^{-1/2} \quad (15)$$

This equation can be used in equation (11) for the calculation of the radius of equivalent circular contact area: Subsequently, the displacement of the equivalent spheres can be found by using equation (9) with the R_{rc} replaced by $2R_e$.

Since no external force is applied on the network, only the weight of the portion of the network above each layer can be considered as the applied force on the contacts in that particular layer. The network is considered to be composed by n layers of equal mass. The weight of each layer can be calculated as follow:

$$w_l = \frac{w_t}{n} \quad (16)$$

However, the force that applied on each layer is not the same across the network. The force applied on any layer will depend on the weight of the layers above. For instance, the bottom layer receives the weight of $n-1$ layers; the second layer receives the weight of $n-2$ layer and so on until the top layer, which receives no force (see Figure 2).

Figure 2: Schematic representation of forces applied on individual fibre layers in a fibrous network.

The average force that is applied on each layer within the network is:

$$F_{av} = \frac{(n-1)}{n} w_l \quad (17)$$

The total applied force on each layer is then equally distributed to all the contacts occurring on the same layer (see Figure 3). Subsequently, the force applied on each contact, per unit mass, can be found through dividing the total weight experienced in that layer by the number of contacts occurring in the same single layer:

$$F_c = \frac{g(n-1)}{\frac{N_{cont}}{n}} \quad (18)$$

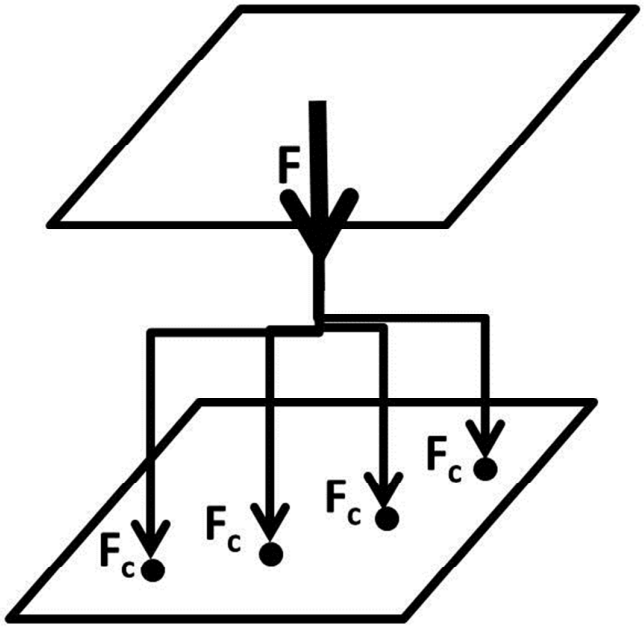

Figure 3: Schematic representation of the force distribution within a single layer. Force, F, represents the overall force applied by the upper layer(s), whereas F_c is the force applied on each individual contact (shown by black t points). Thus, $F = \sum F_c$.

Considering that a contact always occurs between two surfaces, each contact detracts the sum of the two spherical caps in contact. Therefore, the total excluded area at each contact point is:

$$S_{excl} = 2\pi R_e \Delta = \pi a^2 \quad (19)$$

Combining equations (9)-(19) the Hertzian contact area of two cylinders of same material inclined at an arbitrary angle, θ, is given by:

$$S_{excl} = 2\pi \left[\frac{1.06g(n-1)}{2n-1}\frac{R^4}{\sqrt{1-\cos 2\theta}}\frac{\pi+8\lambda\log(1/\varepsilon)}{\log(1/\varepsilon)}\rho_m\frac{1-\nu^2}{E}\right]^{2/3} \quad (20)$$

Equation (20) can be simplified further by introducing an orientation angle factor, Θ, defined as follow:

$$\Theta = \sqrt{1-\cos 2\theta} \quad (21)$$

Since the fibres are randomly oriented within the fibrous network, the probabilities of the contact angle to lie at any value within the range between 0° and 90° are equal.

Thus, an average value for angle factor can be estimated through integration of the term in equation (21):

$$\Theta_{avg} = \frac{1}{91}\int_0^{90}\sqrt{1-\cos 2\theta}\,d\theta \cong 0.89 \quad (22)$$

Using this definition and obtained statistically average value, the average excluded area due to proposed Hertzian contact model within a fibrous network is given by:

$$S_{excl} \cong 2\pi\left\{\frac{1.2(n-1)g}{2n-1}\cdot\frac{[\pi+8\lambda\log(1/\varepsilon)]\rho_m R^4}{\log(1/\varepsilon)}\cdot\frac{1-\nu^2}{E}\right\}^{2/3} \quad (23)$$

2.5. Contact area based on adhesion models

The model developed by Hertz is not universally applicable, since it is subject to certain limitations. In particular it does not take into account adhesion between the two bodies in contact due to various forces of electrostatic/dynamic nature that exist between two surfaces. Different methodologies, such as DMT model[14,15] and JKR model[16], have been developed to include the adhesion effect in the calculation of the contact area. The difference between the two mentioned adhesion models is that the DMT model considers only the adhesive forces acting outside the contact area, whereas the JKR model considers only the forces acting in the contact area[17].

In this study both of these models have been examined and the results are compared with those predicted by aforementioned Hertzian theory.

The radius of the circular contact area predicted by the DMT model is given by:

$$a = \left[\frac{3R_{rc}}{4E}(F + 4\gamma\pi R_{rc})\right]^{1/3} \quad (24)$$

Whereas, the radius of the circular contact area predicted by the JKR model is given by:

$$a = \left[\frac{3R_{rc}}{4E}\left(F_c + 6\gamma\pi R_{rc} + \sqrt{12\gamma\pi R_{rc}F_c + (6\gamma\pi R_{rc})^2}\right)\right]^{1/3} \quad (25)$$

Following the same methodology that has been developed for a Hertzian type contact, equation (23) above can be modified as follow based on the DMT model:

$$S_{excl} = 2\pi\left[\frac{1.19R^2}{E}\left(\frac{g(n-1)[\pi+8\lambda\log(1/\varepsilon)]}{2(2n-1)\log(1/\varepsilon)}\rho_m R^2 + 6.36\pi\gamma\right)\right]^{2/3} \quad (26)$$

and as follow for the JKR model:

$$S_{excl} = 2\pi\left[\frac{1.19R}{E}\left(\frac{g(n-1)[\pi+8\lambda\log(1/\varepsilon)]\rho_m R^3}{2(2n-1)\log(1/\varepsilon)} + 9.53\pi\gamma R + \sqrt{9.53\pi\gamma R\frac{g(n-1)[\pi+8\lambda\log(1/\varepsilon)]\rho_m R^3}{(2n-1)\log(1/\varepsilon)} + (9.53\pi\gamma R)^2}\right)\right]^{2/3} \quad (27)$$

3. Experimental Investigation

3.1. Materials

All the chemical materials were purchased from Sigma-Aldrich and used as delivered. The average molecular weight of PCL was 80,000 gmol^{-1}. Chloroform (CF) and dimethyl sulfoxide (DMSO) had purity of above 98%, whereas for the formic acid (FA) it was above 95%. Cationic surfactant tetrabutylammonium benzoate (TBAB) was also used in the experiments.

3.2. Electrospinning experiments

Horizontal set-up was used for the electrospinning experiments. The polymer solution was forced by a syringe pump (PHD ULTRA, Harvard Apparatus) through a tubing to the metallic needle (18 gauge, 1.270 mm outer diameter, 0.838 mm inner diameter, 3.2 cm length, Fisher Scientific). The high voltage power supply (Series FC, Glassman High Voltage Inc.) provided the electric charge to the needle. Each experiment lasted for about 4 hours. Flat copper plate covered with aluminium foil was used for the collection of the fibres. Table 1 summarises the experimental conditions used in the electrospinning experiments.

Table 1: Experimental conditions used for the production of fibrous networks

Sample	1	2	3	4	5
Solvent system	CF	CF/DMSO	CF/DMSO	CF/DMSO	CF/DMSO
Solvent ratio (% v/v)	73	9/1	9/1	9/1	9/1
Additives	0.2% w/v TBAB	1% v/v FA	-	-	-
Solution concentration (% w/v)	12	12	12	12.5	12.5
Voltage (kV)	25	15	15	25	22
Spinning distance (cm)	15	20	20	17.5	22

Flow rate (ml/h)	2	1	1	2.75	1.41

3.3. Fibre morphology characterisation

Field emission scanning electron microscopy (FESEM, Carl Zeiss (Leo) 1530VP) was used for the measurement of fibre diameter. All the samples were sputter coated by gold (Q150T ES, Quorum) prior to their observation under the microscope. The diameter of the fibres on the images obtained by FESEM was measured by AxioVision software. At least 50 fibre diameters were measured per sample, in order to ensure the accuracy of the measurements. The fibre length was measured using a 30 cm ruler (increments of 1mm). In order to minimise the fibre aggregation effect, the fibres that remained on the collector after the removal of the electrospun mat were used. Those fibres were uncoiled and extended to their full length prior to the measurements. A minimum of 5 measurements were completed for each sample.

3.4. Fibrous network characterisation

All samples were left overnight in a vacuum oven at room temperature for the complete removal of any residual solvent from the production process prior density and SSA measurements. Gas adsorption (ASAP 2020, Micrometrics) was used for the measurement of the electrospun mat specific surface area. Potential gases or vapours absorbed at the sample surface were removed by outgassing the samples. Gas pycnometry (9200 Helium Pycnometer, Micrometrics) was used for the measurement of the electrospun mat density. A digital calliper (ABSOLUTE AOS, Mitutoyo) was used for the thickness measurements of electrospun mats. At least 5 measurements were performed on each mat in order to obtain an average value.

4. Results and Discussion

The design for the experimental testing of the theoretical models involved the production of both, networks composed by porous and non-porous fibres. The former were to be used for the quantification of the pore induction efficiency in terms of surface area increase. The latter were to be used for the determining the contact model that predicts the contact area between the polymer fibres within the network more accurately. This subsequently, results in a more accurate prediction of the overall network specific surface area.

In total five samples were produced, where in two of which the fibres were non-porous and in the remaining three the fibres were porous. The images of the produced fibrous networks are shown in Figure 4.

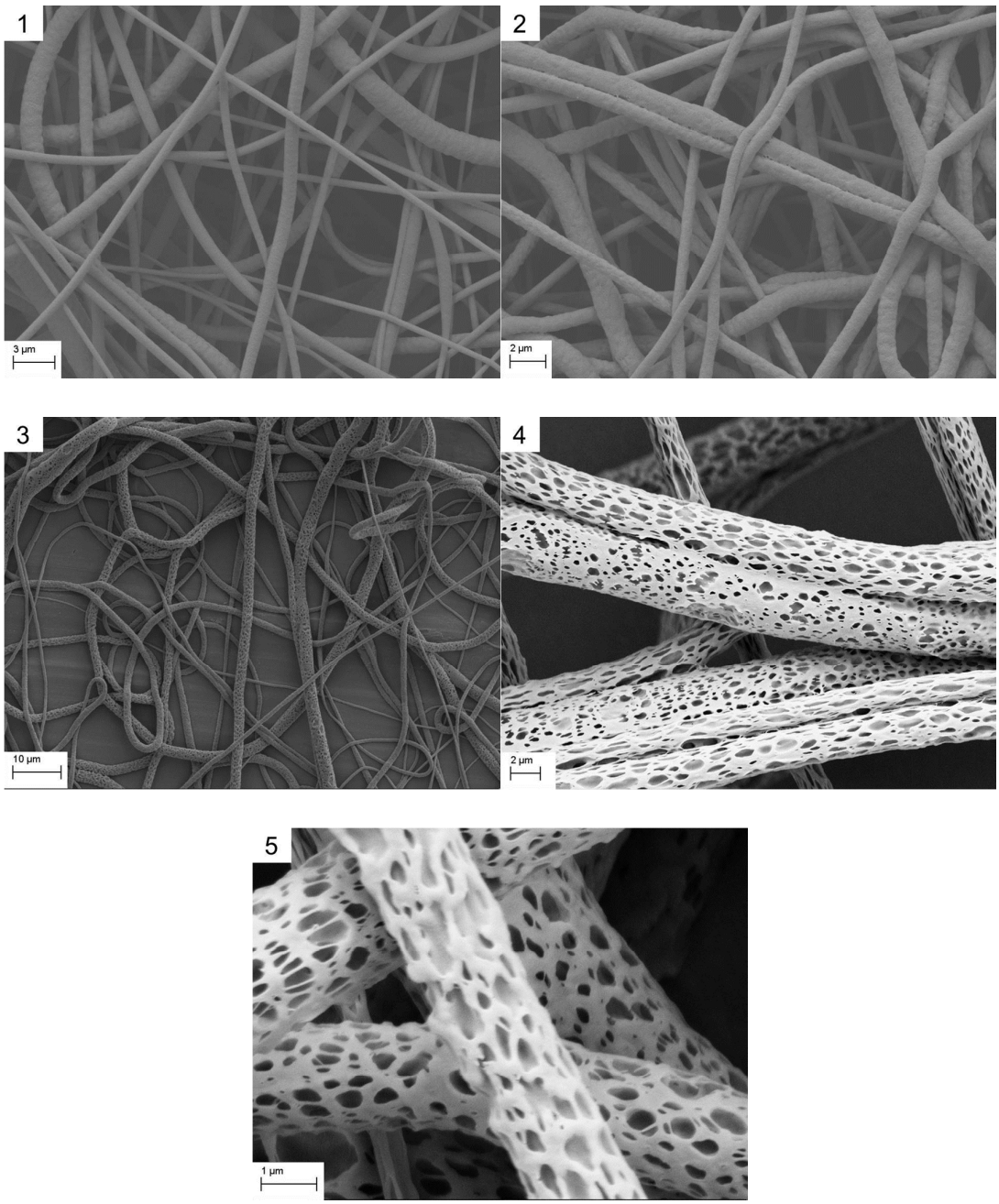

Figure 4: FESEM images of the produced fibrous networks. Numbers on the top left corner represent the sample number

The experimentally measured geometrical and physical properties of individual fibres and the fibrous networks are listed in Table 2.

Table 2: Geometrical and physical properties of the produced fibrous networks (including: network density, ρ, fibre diameter, d, network thickness, t, and fibre aspect ratio, λ, respectively)

Sample	ρ (kg/m^3)	d (nm)	t (mm)	λ
1	987	970	0.47	2110
2	1013	900	0.38	2840
3	1028	1500	0.32	3680
4	910	3310	0.27	2770
5	967	2320	0.41	3130

Network porosity (ε) was calculated using equation (6), the measured network densities (ρ) and the measured value of PCL density (ρ_m=1.155 kg/m^3). The values of the three necessary parameters for the calculation of the theoretical surface area including Young's modulus, Poisson's ratio and polycaprolactone surface tension were obtained from the literature. Croisier et al[18] determined the Young's modulus of electrospun PCL fibres to be approximately 3.7 GPa, whereas the a value of 0.3 has been considered for Poisson's ratio[19,20]. A value of 0.04 J/m^2 was used as the surface tension of polycaprolactone[21]. Table 3 summarises the results predicted by the three theoretical models and the experimentally obtained values for the SSA of the five electrospun fibrous networks.

Table 3: Theoretical predictions based on the three contact models, the theoretical maximum SSA and the experimentally obtained values of the network SSA

Sample	Hertzian model (m^2/g)	DMT model (m^2/g)	JKR model (m^2/g)	Maximum SSA (m^2/g)	Experimental (m^2/g)
1	3.57	2.91	2.19	3.57	2.29
2	3.85	3.36	2.84	3.85	2.73
3	2.31	2.23	2.14	2.31	2.63
4	1.05	1.04	1.02	1.05	1.61
5	1.49	1.45	1.41	1.49	2.15

A reference point was used in order to verify the increase in fibrous network SSA due to pore induction. This point is set to be the maximum SSA that a fibrous network, composed of smooth surface fibres with a given diameter, can achieve as defined by equation (4). Non-porous fibres cannot surpass this threshold and therefore, if the porous fibres were able to exceed this, pore induction would be proven to be a successful technique in terms of increasing SSA. The results of experiments as shown in Figure 5 prove this point.

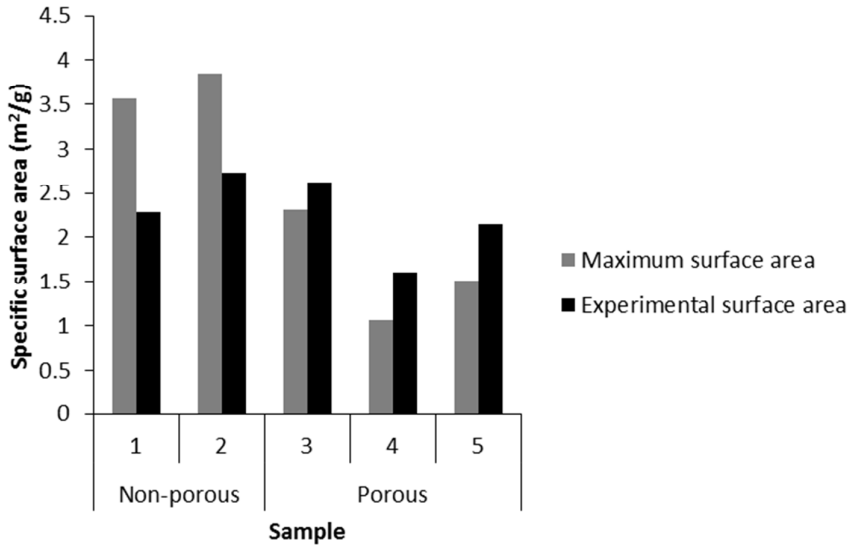

Figure 5: Comparison of the theoretical maximum SSA for the fibrous network with the experimentally observed values. The left column represents the SSA of a network composed by non-porous fibres with diameters equal to the respective experimental diameters

In the case of non-porous fibres the experimentally observed network SSA was always lower than the calculated maximum SSA (by around 36 and 29% for samples 1 and 2, respectively), due to the fibre-to-fibre contacts. In the case of porous fibres, however, the maximum SSA determined experimentally always surpassed the calculated ones by about 14, 52 and 42% for samples 3, 4 and 5, respectively. As was shown in Equation (4), the maximum available SSA is inversely proportional to the density of the material the fibres are composed of. In the case of smooth surface (non-porous) fibres, the fibres are exclusively composed of the polymer and therefore, the fibre network density and the polymer material density match. On the

other hand, in the case of porous fibres, the fibre body is a mixture of polymer and air. Since air is lighter than the polymer, the fibre density is lower compared with the smooth surface fibres and subsequently, the maximum available specific surface area of the network is enhanced.

An interesting observation in Figure 5 is that the SSA of samples 1 and 2 (non-porous) was higher than the SSA of samples 3-5 (porous). That phenomenon was caused by the smaller diameter of the fibres in samples 1 and 2 (< 1 μm) compared to the fibre diameters in samples 3-5 (between 1.5 – 3.3 μm). That highlights the necessity for the consideration of all contributing factors in SSA calculation, since otherwise mislead conclusions might be extracted.

Having verified the increase of the specific surface area following pore induction on electrospun networks, it is essential to also quantify the amount of augmentation. The approach previously presented underestimates the increase in SSA since the excluded surface area due to fibre-to-fibre contacts was not taken into account in the case of the porous network. In order to include this, the most suitable contact model in the investigated samples had to be identified. The Tabor coefficient[22], defined by Equation (28), has been used for such purpose.

$$\mu = \left(\frac{R_e \gamma^2}{E^{*2} {z_0}^3}\right)^{\frac{1}{3}} \quad (28)$$

where, μ is the Tabor coefficient and z_0 is the equilibrium separation between the two surfaces in contact (0.4 nm).

Small values of μ indicate that the use of DMT model is more appropriate, whereas high values indicate that the use of JKR model is more appropriate. The Tabor coefficient values for samples 1 and 2 were calculated to be 139 and 136 respectively, thus the JKR model was expected to describe more accurately the fibre-to-fibre contacts in the network. Indeed, that prediction was verified, as shown in Figure 6.

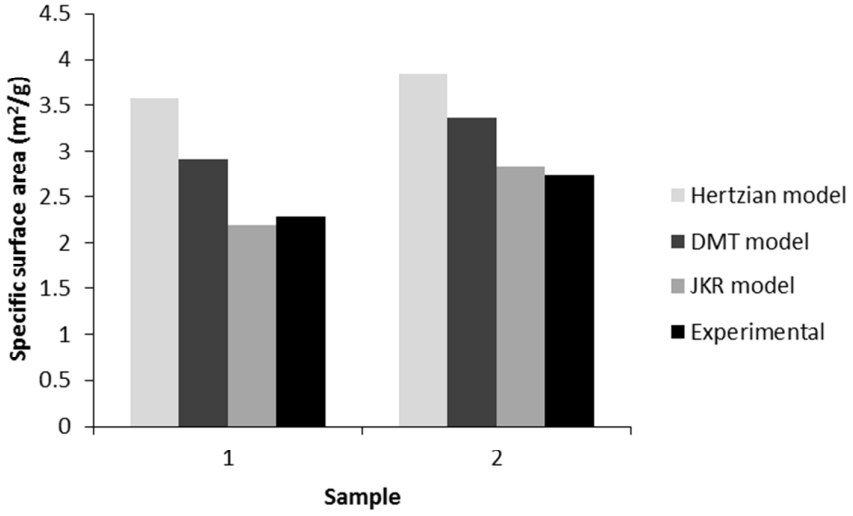

Figure 6: Comparison of the predictions from theoretical models and experimentally observed SSA values for networks composed of smooth surface fibres

In both cases the experimentally obtained values comply with the JKR model. Experimental value of SSA for sample 1 was 2.29 m^2/g (predicted value based on JKR model 2.19 m^2/g), whereas for sample 2 the experimental value was 2.73 m^2/g (predicted value based on JKR model 2.84 m^2/g).

Having verified that the JKR contact model can provide accurate results for the prediction of the polycaprolactone fibrous network SSA, the theoretical values of the SSA for non-porous networks with similar to porous geometrical characteristics were calculated for samples 3, 4 and 5. The results are demonstrated in Figure 7.

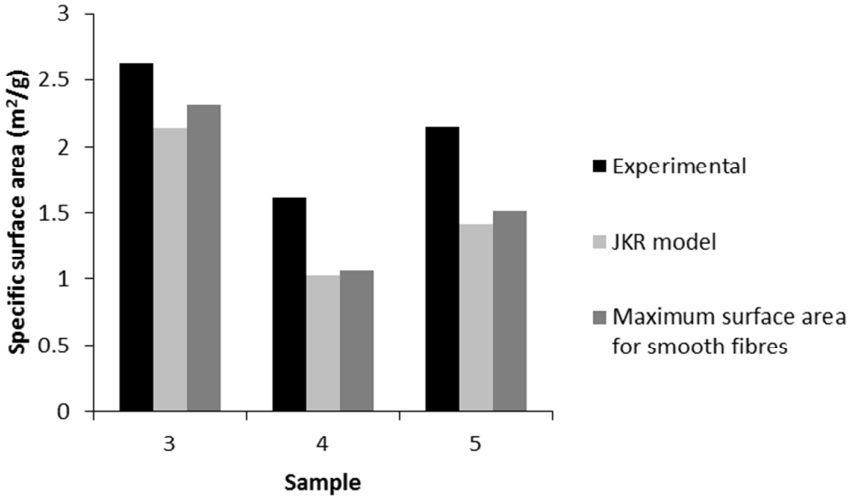

Figure 7: SSA increase due to pore induction. The comparison is made against non-porous networks and considering JKR model for the evaluation of fibre-to-fibre contact areas

Considering the theoretically predicted values, the increase of the network SSA can be calculated as 23, 58 and 52% for samples 3, 4 and 5, respectively. The variance of the SSA increase between samples 3, 4 and 5 can be attributed to the different experimental conditions used for their production[23], which leads to varying levels of pore formation.

It should be noted that the developed models presented in this study are not expected to be universally applicable in electrospun fibrous networks. Phenomena like bead presence on the fibres, varying fibre cross sections (e.g. ribbon), special fibre orientation (e.g. aligned) or incomplete fibre drying are common in electrospinning and should be taken into account in individual cases. Furthermore, the state of the network can be affected by the experimental conditions (e.g. any kind of flow is expected to change the applied force). Nonetheless, the work presented here provides a general methodology and further modifications are certainly required in order to take into account the conditions present under any given circumstances.

5. Conclusions

Increase in SSA of electrospun fibrous network due to pore induction was investigated in this study. Theoretical contact mechanic models based on Hertz, DMT and JKR, correlating the network SSA to its physical properties as well as geometrical characteristics (such as fibre diameter, fibre aspect ratio, network density, and network thickness) were developed. The models offer a more detailed analysis of the factors contributing to the configuration of electrospun network SSA. SSA of networks composed by porous fibres is up to 52% higher than the maximum SSA that non-porous fibres could achieve. JKR model describes accurately the fibre-to-fibre contact area under the experimental conditions used for pore generation. Overall, pore induction was proven, both experimentally and theoretically, to increase the network SSA up to 58%, compared with equivalent non-porous networks.

References

1. Doshi, J.; Reneker, D. H. *J. Electrost.* **1995**, *35*, 151–160.
2. Dods, S.R.; Hardick, O.; Stevens B.; Bracewell D.G. *J. Chromatogr. A* **2015**, 1376, 74–83.
3. Demir, M.M.; Gulgun, M.A.; Menceloglu Y.Z.; Erman, B.; Abramchuk, S.S.; Makhaeva, E.E.; Khokhlov, A. R.; Matveeva, V.G.; Sulman, M.G. *Macromolecules* **2004**, 37, 1787-1792.
4. Casper, C.L.; Stephens, J.S.; Tassi, N.; Chase, D.B.; Rabolt J.F. *Macromolecules* **2004**, 37*,* 573-578.
5. Qi, Z.; Yu, H.; Chen, Y.; Zhu, M. *Mater. Lett.* **2009**, 63, 415-418.
6. Lin, J.; Bin Ding, B.; Yu, J.; Hsieh, Y. *ACS Appl. Mater. Interfaces* **2010**, 2, 521–528.
7. Yu, X.; Xiang, H.; Long, Y.; Zhao, N.; Zhang, X.; Xu, J. *Mater. Lett.* **2010**, 64, 2407–2409.
8. Eicchorn, S.J.; Sampson, W.W. *J. R. Soc. Interface* **2010**, 7, 641–649.
9. Katsogiannis, K.A.G.; Vladisavljević, G.T.; Georgiadou, S. Eur. Polym. J. **2015**, 69, 284-295.
10. Beachley, V.; Wen, X. *Mater. Sci. Eng.* **2009**, C29, 663–668.
11. Eicchorn, S.J.; Sampson, W.W. *J. R. Soc. Interface* **2005**, 2, 309–318.
12. Bagherzadeh, R.; Najar, S.S.; Latifi, M.; Tehran, MA.; Kong, LX. *J. Biomed. Mater. Res., Part A* **2013**, 101A, 2107– 2117.
13. Bhushan, B. Modern Tribology Handbook, Vol. 1, 2001, CRC Press.
14. Derjaguin, B.V.; Muller, V.M.; Toporov, Y.P. *J. Colloid Interface Sci* **1975**, 53(2), 314-326.
15. Muller, V.M.; Derjaguin, B.V.; Toporov, Y.P. *Colloids Surf* **1983**, 7, 251-259.
16. Johnson, K.L.; Kendall, K.; Roberts, A.D. *Proc. R. Soc. London, Ser. A* **1971**, 324, 301-313.
17. Shi, X.; Zhao, Y-P. *J. Adhes. Sci. Technol.* **2004**, 18, 55–68.
18. Croisier, F.; Duwez, A.-S.; Jerome, C.; Leonard, A.F.; van der Werf, K.O.; Dijkstra, P.J.; Bennink, M.L. *Acta Biomater.* **2012**, 8, 218-224.
19. Williams, J.M.; Adewunmi, A.; Schek, R.M.;, Flanagan, C.L.; Krebsbach, P.H.; Feinberg, S.E.; Hollister ,S.J.; Das, S. *Biomaterials* **2005**, 26, 4817–4827.
20. Eshraghi, S.; Das, S. *Acta Biomater.* **2010**, 6(7), 2467–2476.

21. Cava, D.; Gavara, R.; Lagaron, J.M.; Voelkel, A. *J. Chromatogr. A* **2007**, 1148, 86–91.
22. Tabor, D. 1977, *Surface forces and surface interactions*, J. Colloid Interface Sci **1977**, 58, 2-13.
23. Katsogiannis, K.A.G.; Vladisavljević, G.T.; Georgiadou, S. J. Polym. Sci. Part B: Polym. Phys **2016**, 54, 1878-1888.

Table of Contents/Abstract Graphic

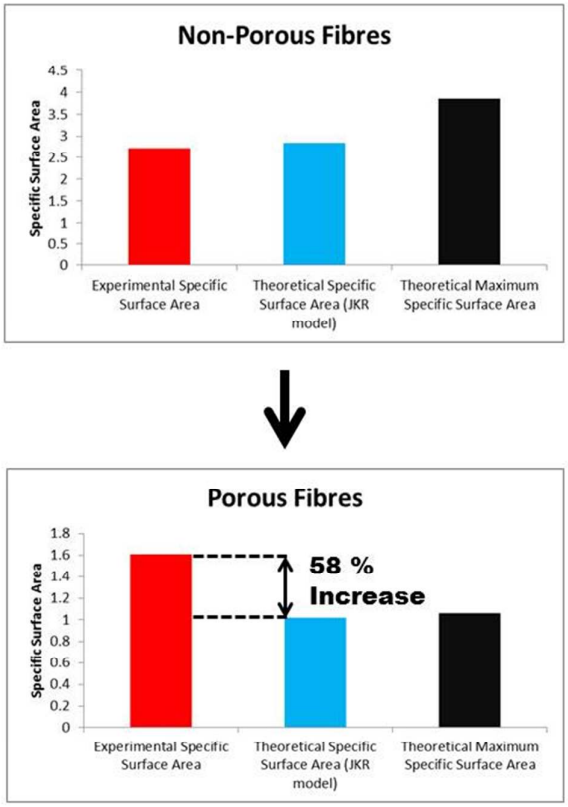

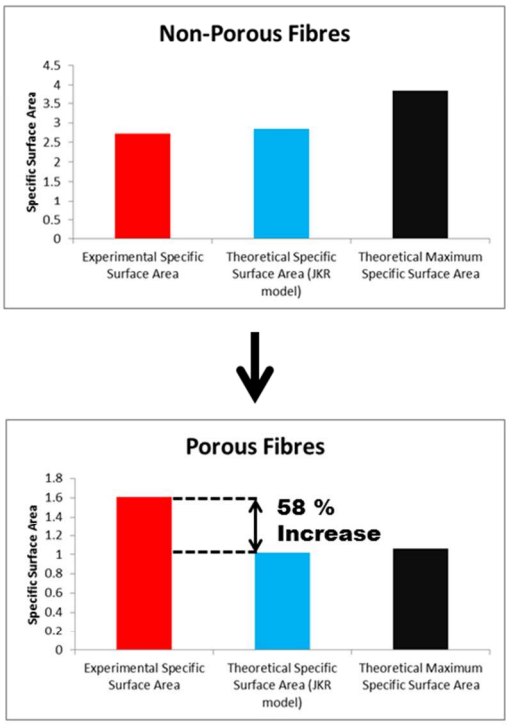

254x190mm (96 x 96 DPI)